

# Assessing Side-Chain Perturbations of the Protein Backbone: A Knowledge-Based Classification of Residue Ramachandran Space

David B. Dahl<sup>1</sup>, Zach Bohannon<sup>2</sup>, Qianxing Mo<sup>3</sup>, Marina Vannucci<sup>4</sup>  
and Jerry Tsai<sup>5\*</sup>

<sup>1</sup>Department of Statistics,  
Texas A&M University,  
College Station, TX 77843,  
USA

<sup>2</sup>Department of Molecular  
and Cell Biology, University  
of California Berkeley,  
Berkeley, CA 94720, USA

<sup>3</sup>Department of Epidemiology  
and Biostatistics, Memorial  
Sloan-Kettering Cancer Center,  
New York, NY 10021, USA

<sup>4</sup>Department of Statistics,  
Rice University, Houston,  
TX 77251, USA

<sup>5</sup>Department of Biochemistry  
and Biophysics, Texas A&M  
University, College Station,  
TX 77843, USA

Received 8 November 2007;  
received in revised form  
20 February 2008;  
accepted 21 February 2008  
Available online  
29 February 2008

Grouping the 20 residues is a classic strategy to discover ordered patterns and insights about the fundamental nature of proteins, their structure, and how they fold. Usually, this categorization is based on the biophysical and/or structural properties of a residue's side-chain group. We extend this approach to understand the effects of side chains on backbone conformation and to perform a knowledge-based classification of amino acids by comparing their backbone  $\phi, \psi$  distributions in different types of secondary structure. At this finer, more specific resolution, torsion angle data are often sparse and discontinuous (especially for nonhelical classes) even though a comprehensive set of protein structures is used. To ensure the precision of Ramachandran plot comparisons, we applied a rigorous Bayesian density estimation method that produces continuous estimates of the backbone  $\phi, \psi$  distributions. Based on this statistical modeling, a robust hierarchical clustering was performed using a divergence score to measure the similarity between plots. There were seven general groups based on the clusters from the complete Ramachandran data: nonpolar/ $\beta$ -branched (Ile and Val), AsX (Asn and Asp), long (Met, Gln, Arg, Glu, Lys, and Leu), aromatic (Phe, Tyr, His, and Cys), small (Ala and Ser), bulky (Thr and Trp), and, lastly, the singletons of Gly and Pro. At the level of secondary structure (helix, sheet, turn, and coil), these groups remain somewhat consistent, although there are a few significant variations. Besides the expected uniqueness of the Gly and Pro distributions, the nonpolar/ $\beta$ -branched and AsX clusters were very consistent across all types of secondary structure. Effectively, this consistency across the secondary structure classes implies that side-chain steric effects strongly influence a residue's backbone torsion angle conformation. These results help to explain the plasticity of amino acid substitutions on protein structure and should help in protein design and structure evaluation.

© 2008 Elsevier Ltd. All rights reserved.

Edited by M. Sternberg

**Keywords:** Ramachandran plot; Torsion angles; Bayesian density estimation; Clustering; Residue backbone similarity

## Introduction

Classification of the 20 amino acids simplifies analysis and helps uncover relationships that are important to protein structure, folding, and function. Such an understanding is especially important in explaining the less-than-straightforward plasticity found between sequence and structure space. Many positions

within a protein sequence can absorb a wide variety of substitutions. In this study, the amino acids are grouped based on the differences and similarities in backbone torsion angle distributions seen in Ramachandran plots.<sup>1</sup> As shown previously, Ramachandran plots provide a simple and direct evaluation of the main chain's conformational space.<sup>2,3</sup> In this work, we take a knowledge-based approach to amino acid classification and measure the similarity that the various side-chain functional groups have upon the conformation of the main-chain polymer.

Typical classification of amino acids has naturally focused on the side chain or the portion of a residue

\*Corresponding author. E-mail address: [jwtsai@tamu.edu](mailto:jwtsai@tamu.edu).  
Abbreviations used: H, helix; E, sheet; T, turn; C, coil;  
PDB, Protein Data Bank.

that is different, since the main chain is a repetitive polymer. The most straightforward method has been the use of the chemistry of an amino acid, such as hydrophobicity,<sup>4</sup> in grouping amino acids. However, the size, shape, and chimeric chemistry of some side chains complicate such chemical classification. For example, the side chain of Lys is considered a charged group, but the positive charge follows a long nonpolar chain of four carbon atoms. On the other hand, Trp is a bulky aromatic group with some hydrophilic tendencies, but this side chain is often considered a large hydrophobic residue. Using these hydrophobicity-based groupings to reduce the amino acid alphabet, insights into protein design have been made in structure/folding,<sup>5</sup> as well in as enzyme catalysis.<sup>6</sup> Computational/knowledge-based approaches have also been used to group amino acids.<sup>7–10</sup> Such clustering of amino acids has been used to improve sequence alignments,<sup>11</sup> as well as remote homolog detection.<sup>12,13</sup>

In this work, we approach amino acid clustering from a classic structural point of view based on  $\phi, \psi$  backbone distributions, which has been performed previously.<sup>14–17</sup> Taking this analysis a step further, we increase the resolution of this analysis by also making classifications based on four secondary structure types: helix (H), sheet, (E), turn (T), and coil (C). To make accurate comparisons between different residues' Ramachandran plots, we must first overcome the sparse and discontinuous sampling of  $\phi, \psi$  space in the Protein Data Bank (PDB).<sup>18</sup> Even though information on known structures is substantial<sup>19</sup> in the PDB, it is not enough to adequately sample backbone torsion angle space for all residues,<sup>16</sup> especially when the data are further divided into secondary structure types. Several approaches have been used to address this sampling problem. The simplest have been 1) to use a large set of PDB structures,<sup>14</sup> which oversamples certain folds and therefore regions of  $\phi, \psi$  space, and 2) an increased bin size of  $10^\circ \times 10^\circ$  or larger,<sup>14–17</sup> which also reduces resolution and accuracy. Another approach is to smooth the data using basic interpolation,<sup>20</sup> a Gaussian approximation,<sup>16</sup> or an empirically derived density-dependent mask.<sup>21</sup> When the data become too sparse, smoothing unknown values becomes less reliable. In this work, we consider Bayesian density-estimated representations of a residue's  $\phi, \psi$  distributions to deal with the sparsity of data. Such modeling allows meaningful comparisons between Ramachandran plots and is particularly effective for analyses classified by secondary structure, where data are even sparser. A Bayesian-based approach has been used previously<sup>22</sup> on the complete backbone torsion angle space. Unlike our objective of modeling continuous densities from sparse data, the goals of their Fourier-based statistical formulation were to avoid oversampling regions of the Ramachandran plot and to produce a single well-behaved distribution for use as a statistical potential function. In this work, we model all 20 amino acids (as well as their four separate secondary structure classes) by taking a non-parametric Bayesian approach with a Dirichlet pro-

cess mixture model that recognizes the uncertainty in the number of components and allows it to vary. This estimation in our model is simple and can be carried out via standard computational methods. The results of this modeling allow us to investigate the backbone propensities at a finer resolution of individual secondary structures. As an example, we cluster residues based on their  $\phi, \psi$  distributions and infer constructive insights into the relationship between protein sequence and structure. In effect, by grouping on the  $\phi, \psi$  torsion angle distributions, we are able to investigate the influence of the side chain on its respective backbone's accessible conformational space.

## Results and Discussion

As described in Materials and Methods, backbone torsion angles were calculated from a set of non-redundant protein structures and classified in the following ways. First, the  $\phi, \psi$  angle pairs were grouped according to amino acid, which will be further referred to as the All set for simplicity. Then, for each amino acid, the angles were separated according to four classes of secondary structure using the Definition of Secondary Structure for Proteins program. In this work, the following shorthand will be used to reference these sets: helix (H), sheet (E), coil (C), and turn (T). This approach resulted in five groupings of the data per amino acid. The raw  $\phi, \psi$  angles are shown as gray points in the Ramachandran plots for the amino acid Ala in Fig. 1. Next, the distributions of these torsion angle sets were calculated either by binning or by Bayesian non-parametric estimation. Contour representations of the density estimates for Ala are reported in Fig. 1, overlaid on the raw data. These highlight the most populated areas in the plots (i.e., the modes of distribution). For Ala, there are values in all four types of secondary structure, although H is dominant in the All plot. Separating the data into the four individual secondary structure elements allows us to see the local effect of each side chain on their respective backbones. In general, for all 20 amino acids, the distributions were similar to those shown in Fig. 1, except for the well-known differences from Gly and Pro. With only a hydrogen atom as a side-chain group, Gly exhibits the most flexibility in backbone conformation and very broad distribution of  $\phi, \psi$  angles, whereas Pro is the most constricted in  $\phi$  due to its side chains' covalent ring structure involving its main-chain nitrogen. As expected, the H class is the best-defined class of the four secondary structure classes and is followed by T class. The E and C classes display similar variations, although the C class is less well populated.

### Binning versus density estimation

The simplest approach to estimating distributions is to bin the data. However, in many cases, the data are sparse and the binning method results in coarse estimates subject to random fluctuations. We

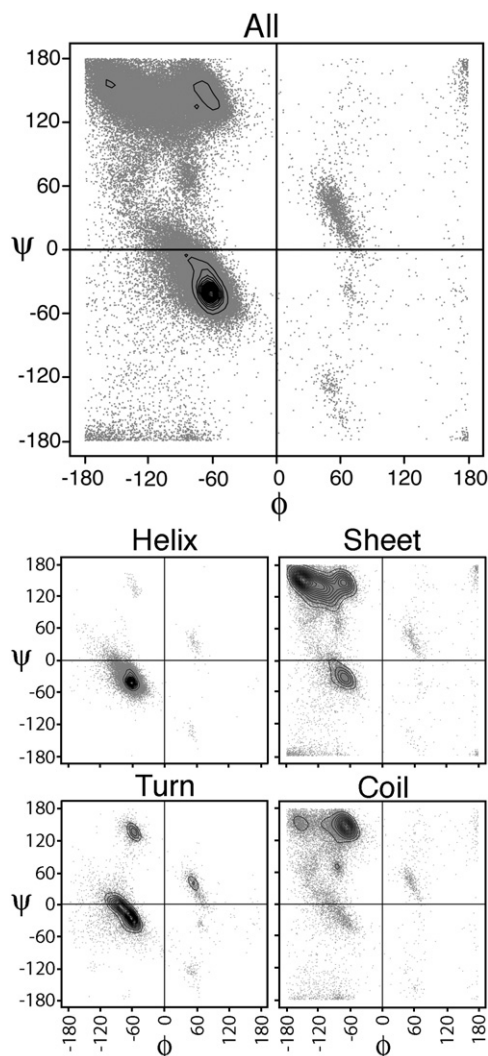


**Fig. 1.** Ala Ramachandran plots of the five classes. Raw torsion angle data are shown by gray dots, while density-estimated distributions are overlaid using contour representations. Distribution classes are labeled above their respective plots. The highest peak in the All and helix (H) distributions occurs at  $(-65^\circ, -40^\circ)$ . This peak is at  $(-150^\circ, 150^\circ)$  for sheet (E), at  $(-65^\circ, -20^\circ)$  for turn (T), and at  $(-70^\circ, 140^\circ)$  for coil (C).

therefore used a Bayesian nonparametric approach to generate estimates (see Materials and Methods). Because these estimates only considered the data bounded from  $180^\circ$  to  $-180^\circ$ , we wanted to ensure that we were reproducing the periodic boundary at  $180^\circ/-180^\circ$  correctly. As a check of our estimated distributions, the distance between the binned and the density-estimated  $\phi, \psi$  torsion angle distributions was calculated. Divergence scores ranged from 0.017 to 0.247. The top panel of Fig. 2a shows this comparison for each of the five classes described above, while the bottom panel of Fig. 2a depicts the number of  $\phi, \psi$  observations for each amino acid and class. While H class is the most populated overall, the amino acids branched at the  $C^\beta$  atom (Val, Ile, and Thr) favor E class, as expected. Coil is well

populated, whereas T class has the least number of members. By combining the analyses in both parts of Fig. 2a, we found, as expected, that the number of observations correlates with distance divergence: more observations produced lower divergence scores and vice versa. Figure 2b provides examples of this relationship. The upper portion of Fig. 2b contrasts the binning and the density-estimated distributions from the most populated class Leu All with the lowest distance divergence. In such a well-sampled case, the distributions are very similar to each other. Both show the same peak in the helical area, with a slight variation in the connection of the distribution over the sheet/coil region. This demonstrates that our Bayesian density estimation method closely matches the simpler binning approach when data are plentiful. The lower portion of Fig. 2b shows the same comparison for the least populated case and the second highest divergence distance of Trp T class. The binned distribution on the left is clearly uneven and rather coarse, whereas the Bayesian density estimation produces a regular smooth distribution that models well the diversity in the data, while the binned distribution is informative, making comparisons problematic for such irregular distributions. In the Bayesian density estimation, the left- and right-handed conformations are identified, and the sheet-like angles are also found. In both cases, the  $180^\circ/-180^\circ$  boundary is reproduced, although most of the data fall away from the periodic boundary. Overall, these results demonstrated that our Bayesian estimation method faithfully represents the distribution of data and produces smooth estimates to permit more natural comparisons.

### Density-estimated distributions

While the distributions are similar, there are perceptible and significant differences. Overall, the density-estimated distributions cover the expected areas of the Ramachandran plot,<sup>23,24</sup> and, as expected, the disallowed regions<sup>25</sup> are not well sampled. The peaks fall into the well-known regions of the Ramachandran map.<sup>21</sup> Each secondary structure class will be discussed individually.

#### H class

For the H class, the differences between amino acids is primarily in the shape of the distribution that resides in the  $\alpha$  region (Fig. 1). The peaks range in value between  $-60^\circ$  and  $-65^\circ$  in  $\phi$  and between  $-40^\circ$  and  $-45^\circ$  in  $\psi$ . Of all the classes, this H class exhibits the most consistent distributions. The only exception is for Pro, which is restricted in  $\phi$  and produces a peak lower of  $-55^\circ, -35^\circ$  in  $\phi, \psi$  value. For the remaining classes, peak and distribution shape are both factors in the clustering.

#### T class

The T class is most similar to the H class (Fig. 1), but has a broader distribution and additional strong

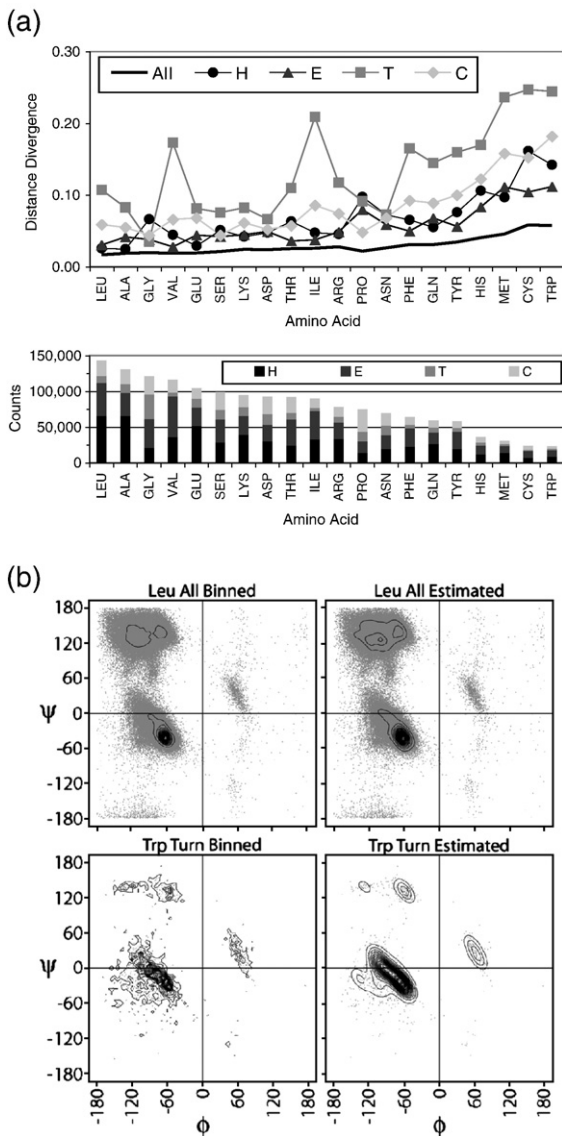


**Fig. 2.** Comparison of binning *versus* density estimation. (a) Top line graph shows the distance divergence between the binned and the Bayesian density estimation representations of the Ramachandran plots for each of the 20 amino acids in each of the five classes: All, H (helix), E (sheet), T (turn), and C (coil). Bottom stacked histogram shows the number of observations for each class, where the stacked total is the number of observations for the All class. (b) Ramachandran plots are shown for the distributions with the highest number (Leu All) and the lowest number (Trp T class) of observations. Data points are shown in gray, and the calculated distributions are shown by the contour lines. Binned estimates are on the left, and Bayesian density estimates are on the right.

peaks in the left-handed helical region. In direct comparison to the H class, the T-class peaks are consistently more negative in  $\phi$  and more positive in  $\psi$ , and therefore move to the left and up in the Ramachandran plot towards the  $3_{10}$  helical conformation. This is even so for Pro. In this class, the exception is Gly, which shows a primary  $\phi, \psi$  peak of  $80^\circ, 10^\circ$  in the left-handed helical region. Generally,

the other clusters also have secondary peaks in the left-handed helical region. For example, the Asn, Asp cluster's second peak at  $\phi, \psi$  is  $55^\circ, 40^\circ$ .

### E class

In the E class, the distributions are shaped more broadly, with major peaks in the upper left region of the Ramachandran plot ranging from  $-95^\circ$  to  $-150^\circ$  in  $\phi$  and from  $125^\circ$  to  $155^\circ$  in  $\psi$  (Fig. 1). Secondary peaks are located around the poly-Pro region, with a  $\phi$  around  $-65^\circ$  and with similar  $\psi$  values as the major peak. As before, the Gly peak of  $80^\circ, 10^\circ$  is in the left-handed helical region at  $\phi, \psi$ , but has many values in the classic upper left E region of the Ramachandran plot. Closer inspection reveals that these values are due to Gly at the ends of  $\beta$ -sheets. As expected, being restricted in  $\phi$ , the Pro peak in the E class is centered in the poly-Pro region at  $-65^\circ, 145^\circ$ .

### C class

Although covering the same region, the C-class distributions are also broad (Fig. 1). In comparison to the E class, the C-class peaks are located in the poly-Pro region. They are smaller and less varied in  $\phi$  ( $-65^\circ$  to  $-95^\circ$ ) but similar in  $\psi$  ( $135^\circ$  to  $155^\circ$ ). These peaks are moved over slightly to the right. Thr and Gly are exceptions, with higher  $\psi$  values of  $165^\circ$  and  $170^\circ$ , respectively, but with secondary peaks in the poly-Pro region. Once more, Pro is restricted to the  $\phi$  value of  $-65^\circ$  and centered in the poly-Pro region.

As a composite of the four secondary structure classes, the All class is more complicated and exhibits all the characteristics described above, although the highest peak is usually in the right-handed helical region.

### Clustering within classes

For each class (All, H, E, C, and T), divergence distances were calculated and used to cluster the 20 amino acids. Table 1 summarizes the resulting clusters. As shown in Table 1, clusters were taken when one of two criteria were met: (1) all the amino acids were in clusters of at least two members besides Gly and Pro, and (2) the clustering distance became larger than the lowest divergence distance to a distribution in another class. This was performed since the Gly and Pro distributions are so different from all the others. The divergence scores for Gly and Pro clearly separate these distributions from the others, which is expected. Without a side-chain group, Gly is flexible and populates all quadrants of the map. In contrast, Pro is restricted in  $\phi$ , since the side chain makes a covalent bond with the backbone nitrogen. Their difference from all the other distributions, even within each class, is very evident in Fig. 3, where a tree diagram shows the similarity relationship between the four secondary structure classes. Figure 3 clearly shows that the H class exhibits the smallest divergences between residues, which clusters at

0.021 in Table 1. T, C, and E classes cluster at 0.045, 0.048, and 0.051, respectively. The All class has the highest value at 0.064.

In general, the amino acids group, in certain cases, according to similar biophysical characteristics, but there are some interesting exceptions. Since it combines all the secondary structure types, the All class will be used as a reference point. The All class produced six clusters, and they will be described from the most different to the most similar (bottom up). The two singleton clusters are Gly and Pro, as expected. Next is a group that combines the residues with planar delocalized rings (aromatics Phe, Trp, and Tyr with imidazole His) with the hydroxyl-containing residues (Ser, Thr, and again Tyr) and Cys. For reasons made clearer in the discussion of the clusters within secondary structure classes, this cluster is named the aromatic group. Asn and Asp make up the next cluster and are similar in shape and chemistry, differing by a replacement of an oxygen in Asp by an amide in Asn. Asp is usually charged, while Asn is polar. Following known conventions, this group is termed the AsX group. For the same reason, Gln and Glu also group together, but always with other amino acids. The reason for this is that the Gln distribution is more similar to the Met distribution, while the Glu distribution is more similar to the Arg distribution. This group usually also includes Lys and sometimes Leu. This resulting group is a mix of hydrophobic (Leu, Ala, and Met), polar (Gln), and charged (Arg and Lys) residues. Structurally, they are mostly longer side chains, except for Ala, and none is branched at the C<sup>β</sup>, although this also pertains to other previous clusters; thus, this group will be termed the long cluster. The most similar cluster consists of the hydrophobic Ile and Val, and will be termed nonpolar/β-branched. Both are branched at their side-chain C<sup>β</sup> atoms, but differ in that Ile is longer by a methylene group. Surprisingly, the other C<sup>β</sup>-branched residue Thr is not in this group, although Thr is very different chemically with a hydroxyl group.

In comparison to previous classifications, our clusters shown in Table 1 are similar to the Gly and Pro singletons and the AsX group, but there are significant differences. For the smaller structure set and 20° × 20° binning,<sup>15</sup> Ile and Val are found grouped like ours, but His and Cys are singletons, and one large cluster combines our aromatic and long clusters together. This is most likely due to the smaller sample size available at the time of the study, where certain distributions did not have enough data to show their true distribution. For the study based on a larger structure set and/or a broader 10° × 10° binning,<sup>14</sup> there are similarities where our results concur on the singletons of Gly and Pro, as well as the AsX group (Table 1). We differ in that our analysis does not include Thr with Ile and Val, but instead clusters with the hydroxyl-containing residues. The long cluster is similar, but ours also includes Ala, Gln, and Met. We also include all the aromatics together. These differences are due pri-

**Table 1.** Amino acid clusters

All	Helix			Turn			Sheet			Coil		
	Number	Cluster	Distance <sup>a</sup>	Cluster	Distance <sup>a</sup>	Peak φ ψ	Cluster	Distance <sup>a</sup>	Peak φ ψ	Cluster	Distance <sup>a</sup>	Peak φ ψ
1	Ile Val	0.015	0.004	Ile Val	0.010	-65 -45	Ala Ser	0.028	-145 -153	Phe Tyr His Cys	0.020	-70 140
2	Glu Met Gln Arg Lys Leu Ala	0.027	0.009	Met Leu Gln Arg Glu Lys Ala Ser	0.024	-65 -40	His Cys Lys Glu Gln Arg Thr	0.028	-127 142	Ile Val	0.020	-75 130
3	Asn Asp	0.029	0.014	His Phe Tyr	0.029	-62 -43	Asn Asp	0.033	-98 118	Gln Lys Met Arg Glu Trp Leu	0.021	-73 144
4	Phe Tyr Trp Cys His Ser Thr	0.039	0.015	Thr Trp	0.038	-63 -43	Ile Val Leu	0.035	-117 127	Asn Asp	0.029	-80 120
5	Gly Pro	-	0.018	Thr Trp Pro	0.047	-65 -40	Gly	-	85 10	Ala Ser	0.045	-73 150
6		-	-	Pro	-	-65 -40	Pro	-	-65 145	Thr	-	-85 165
7		-	-	Gly	-	-65 -40	Gly	-	80 10	Pro	-	-85 150
8		-	-	Pro	-	-55 -35	Pro	-	-	Gly	-	-80 170

<sup>a</sup> Average distance divergence of the cluster.

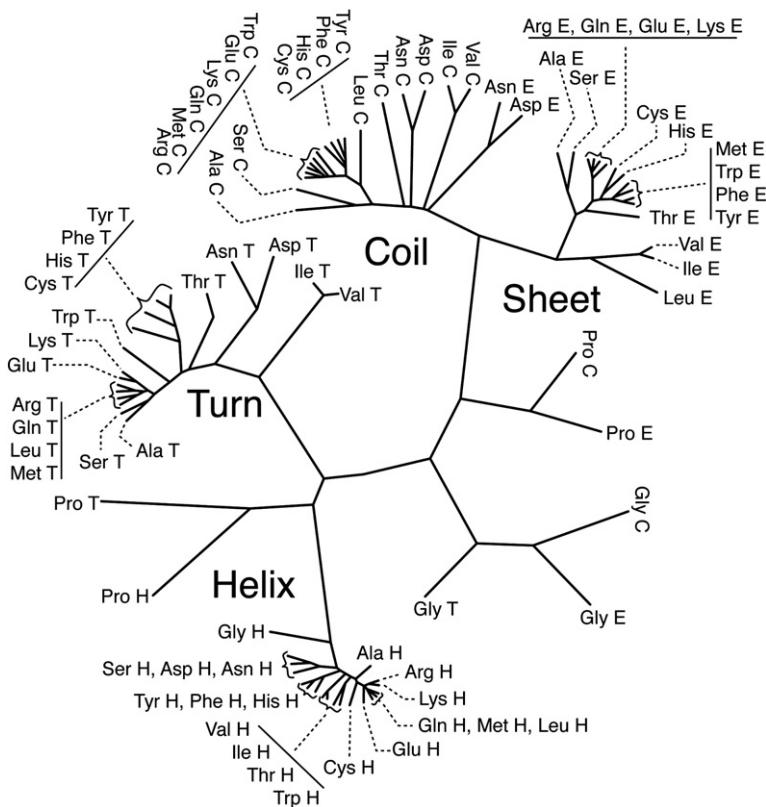


**Fig. 3.** Unrooted tree diagramming the relationship between the density-estimated Ramachandran distributions of the four secondary structure classes H (helix), E (sheet), C (coil), and T (turn). The tree was drawn with the DrawTree program from the Phylip package<sup>26</sup>, where the lengths of the branches are an indication of the divergence distance between two distributions.

marily to our smaller sampling bins that capture finer details. In addition, we were more rigorous in our structure set, so that we could avoid oversampling especially in the helical area. As can be clearly seen, the helical region contains most of the density in the All distributions and, therefore, can dominate any comparisons. For this reason, we performed the same analysis using the four secondary structure classes.

For the four secondary structure classes, Gly and Pro are always independent clusters as a result of our cutoff criteria, but this is reasonable considering their very dissimilar distributions. Although Gly can have very broad distributions, Gly can be restrained especially in the H class, where Gly is most similar to the Glu distribution at 0.042. In the T class, the Gly distribution produces its worst comparisons, with Pro at 0.514 and Val at 0.465. Being restricted in  $\phi$ , the Pro distributions are very different and are no more similar than 0.137 in the T class with Ala. In addition, except for the C class, where it is the third worst, the Pro distributions are involved in the highest divergences for all classes, where the overall worst value is 0.517 between Ile and Pro in the E class.

Among those remaining, the most consistent clusters across the four secondary structure classes are the nonpolar,  $\beta$ -branched, and AsX clusters. The nonpolar/ $\beta$ -branched pair is strongly similar in H and T classes. In C class, they are the second most similar; in E class, they are interestingly joined by Leu. In the E, C, and T classes, AsX clusters as the pair, but in the H class, it is joined by Ser. The aromatic class splits into the T and C classes as Phe,

Tyr, His, and Cys. In the H class, the aromatic class is composed of only His, Phe, and Tyr; in the E class, the aromatic class joins the long class. The long class is the same as in the T class, but loses Ala and Ser in the H and C classes. Interestingly, the long and aromatic clusters are joined in the E class. As for other interesting clusters, the Ala distribution's strong helical content puts it in a singleton cluster in the H class. For E and C classes, Ala pairs with Ser, although these are small and only differ by the addition of a single hydroxyl to Ser. In the H and T classes, Thr and Trp are independent of the aromatic cluster. Since Thr is  $\beta$ -branched and Trp is large, these could be considered bulky. In the C class, Trp joins the long cluster and Thr is a singleton mostly because Thr has such a broad distribution with a strong density around  $\psi$  values of  $170^\circ$ .

Overall, this clustering of amino acid Ramachandran distributions between the various secondary structure classes suggests the following general groupings: nonpolar/ $\beta$ -branched (Ile and Val), AsX (Asn and Asp), long (Met, Gln, Arg, Glu, Lys, and Leu), aromatic (Phe, Tyr, His, and Cys), small (Ala and Ser), bulky (Thr and Trp), and, lastly, the singletons of Gly and Pro. Although most stay within their group, a number (Ala, Cys, Leu, Ser, Trp, and Thr) cluster differently, depending on secondary structure class.

### Clustering between classes

Using the distance divergence, the amino acid distributions from each of the four secondary

structure classes were also clustered against each other, and the results are shown by the tree diagram in Fig. 3. Except for H class, Gly and Pro distributions separate themselves from the other amino acids, yet somewhat follow the secondary structure classes. The most different are the Gly distributions in C, E, and T classes that group together and away from all the other distributions. Although also separate from the other amino acids, the Pro distributions mimic the overall class distributions in that E and C classes are closer together, and H and T classes are closer together.

For the remaining 18 amino acids, the secondary structure classes group together. As stated before, the H class is the most similar cluster and even includes Gly. The T class is more similar to the H class than to the E class or the C class. Likewise, the E and C classes are more similar to each other than to the H class or the T class. The clusters described in Table 1 can clearly be seen in this diagram. In each secondary structure class, the nonpolar/ $\beta$ -branched and AsX clusters clearly group together and away from the other groups. In addition, the diversity in distributions based on secondary structure types can be seen. While the broadest class looks to be the T class, the E-class distributions of Asn and Asp actually cluster closer to the C class, which explains why the E class is the broadest. It is interesting to note that there is no more overlap between secondary structure classes. This result indicates how distinct these types of protein structure are even though they sample similar regions of torsion angle conformational space.

## Conclusion

As shown in Figs. 1 and 2, the Bayesian nonparametric density estimation allows us to provide a reasonable approximation of a Ramachandran distribution especially when the data are sparse. This result is particularly satisfying, as our density estimations were made without including periodicity. Comparisons to a periodic treatment that we are now developing show no significant differences for the data analyzed in this paper (K. Lennox, D. Dahl, M. Vannucci & J. Tsai, Density estimation for protein conformation angles using a Bivariate von Mises distribution and Bayesian nonparametrics, unpublished results) (see Materials and Methods). Using a distance divergence metric, the distributions can now be consistently compared and clustered for all 20 amino acids, as well as for their respective secondary structure classes. The result is a higher-resolution scheme for classifying amino acids based on their differences in sampling backbone conformational space. Although calculation of main-chain torsion angles examines a regular polymer of repeating atoms, the similarities/differences between the plots must be attributed to the individual influences of side-chain functional groups on their respective backbones. As with any knowledge-based clustering, the data dictate the results, which

do not always follow expectations. For example, the groupings themselves do not suggest that two amino acids such as Thr and Trp are similar in chemistry, but the analysis shows that they both affect the backbone in the same manner. The theme for the clusters seems to be less about their chemistry and more about their shape or sterics. It follows that the principal effect of the side-chain group on the backbone is steric, since the chemistry (polarity/charge) would be difficult to bring to bear on a residue's own main-chain atoms. Therefore, this analysis shows that side chains affect the backbone according to seven types: nonpolar/ $\beta$ -branched (Ile and Val), AsX (Asn and Asp), long (Met, Gln, Arg, Glu, Lys, and Leu), aromatic (Phe, Tyr, His, and Cys), small (Ala and Ser), bulky (Thr and Trp), and, lastly, the singletons of Gly and Pro. As with any categorization of amino acids, there are caveats such as the behaviors of Ala, Cys, Leu, Ser, Trp, and Thr in certain secondary structure classes.

These results certainly do not take the place of the most common classification of protein side chains. In particular, these results have very little bearing on the nonlocal tertiary environment that is effected upon amino acid change. Instead, these results can explain why point mutations in many cases have no effect on the structure or function of a protein. In other words, the results from our clustering provide the explanation that the side-chain functional groups affect their backbone conformations in a similar fashion. For example, in terms of substitution matrices such as BLOSUM62,<sup>27</sup> our clustering helps to explain the somewhat surprising yet favorable substitution pairs such as Glu/Lys, Ala/Ser, and His/Tyr. In fact, similar work has been used to create amino acid substitution matrices,<sup>15,16</sup> which have been useful for identifying structurally similar regions between proteins. In this work, we are focused more on the structural implications of these results and find that amino acids substitutions do not drastically perturb the allowable backbone conformational space upon mutation, excluding Gly and Pro. On the contrary, the closeness of the distributions, as seen in Fig. 3, implies that mutation to another residue changes the range of possible main-chain conformations at a position and allows protein structures the potential for evolutionary change. Such conclusions have impact not only on the understanding of protein evolution but also on the use of amino acid substitutions in protein structure prediction (specifically template-based modeling), as well as protein design.

## Materials and Methods

In biochemistry, a torsion angle or a dihedral angle is defined by four atoms connected by three covalent bonds and describes the rotation around the central bond of the outer two bonds with respect to each other. Because the backbone of a protein structure in its most simplest form can be described as a covalent polymer made up of three repetitive atoms per residue (nitrogen N,  $\alpha$  carbon C $^\alpha$ , and

carbonyl carbon C), torsion angles must involve more than one residue. For reference, the  $i$  subscript refers to the relative position in the protein chain. There are three backbone torsion angles. The  $\phi$  angle consists of the atoms  $C_{i-1}$ ,  $N_i$ ,  $C_i^\alpha$ , and  $C_i$ . The  $\psi$  angle consists of the atoms  $N_i$ ,  $C_i^\alpha$ ,  $C_i$ , and  $N_{i+1}$ . The last angle  $\omega$  consists of the atoms  $C_i^\alpha$ ,  $C_i$ ,  $N_{i+1}$ , and  $C_{i+1}^\alpha$ . The first two angles range over  $360^\circ$ , but the convention is to report values between  $-180^\circ$  and  $180^\circ$ . The third torsion angle  $\omega$  is usually fixed at  $0^\circ$  (less so) and  $180^\circ$  (more so) due to resonance and partial double bond characteristics.<sup>28</sup> For this reason, our study will not include statistics on  $\omega$  and will concentrate on the variation found in residue  $\phi, \psi$  torsion angles.

### Data set

Our data set of nonhomologous structures was generated from the PISCES server<sup>29</sup> generated from the May 20, 2003 release of the PDB, using the following criteria: percent identity  $\leq 50\%$ , resolution of 0.0–2.5 Å, and  $R$ -factor  $< 1$ . Only X-ray entries were considered. The resulting list of 6702 separate protein chains is available upon request.

### Structural analysis

A C program that calculates the backbone  $\phi, \psi$  torsion angles of residues in a protein chain in the following manner was written. To avoid complications from variations in bond angles, the actual torsion angle is calculated as the angle between the normals of two planes, as performed classically.<sup>1</sup> The  $\phi$  angle is computed between the normal-to-plane made by three atoms  $C_{i-1}$ ,  $N_i$ , and  $C_i^\alpha$  and the normal-to-plane made by the three atoms  $N_i$ ,  $C_i^\alpha$ , and  $C_i$ . The  $\psi$  angle is calculated between the normals made by the  $N_i$ ,  $C_i^\alpha$ ,  $C_i$  plane and the  $C_i^\alpha$ ,  $C_i$ ,  $N_{i+1}$  plane. Since no residue precedes the first residue, it lacks a  $\phi$  angle. Similarly, the last residue lacks a  $\psi$  angle without a residue following it. Therefore, these residues were excluded from the calculation. The output consists of the amino acid, its  $\phi, \psi$  torsion angle pair, and secondary structure as defined by the Definition of Secondary Structure for Proteins program.<sup>30</sup> The normal eight classes were condensed into four: helices (H), sheets (E), coils (C), and turns (T). This output was used as the raw data from which all statistics were calculated.

### Data binning

The binning method estimates the torsion angle density as simply a bivariate step function whose value is constant in  $5^\circ \times 5^\circ$  squares. Its value within the square is proportional to the number of  $\phi, \psi$  pairs in the data set that fall into that square. Since each axis range spans  $360^\circ$ , there are a total of  $(360/5)^2 = 5184$  squares.

### Nonparametric Bayesian density estimation

The backbone torsion angles  $\phi, \psi$  calculated from the PDB and classified based on amino acid and secondary structure type (see above) can be viewed as samples from the joint distribution of the  $\phi, \psi$  torsion angles. We estimated the joint distribution of the  $\phi, \psi$  torsion angles using Bayesian nonparametric density estimation.<sup>31,32</sup> For a particular grouping of torsion angles based on amino acid and secondary structure, suppose we have  $n$  entries in the PDB (i.e.,  $n$  pairs of angles measured in degrees ranging

from  $-180^\circ$  to  $180^\circ$ ). We propose the following Dirichlet process mixture model:

$$(\phi_i, \psi_i) | \mu_i, \lambda_i \sim F((\phi_i, \psi_i) | \mu_i, \lambda_i) \quad (1)$$

$$\mu_i | G(\mu) \sim G(\mu) \quad (2)$$

$$\lambda_i | H(\lambda) \sim H(\lambda) \quad (3)$$

$$G(\mu) \sim DP(\eta_0 G_0(\mu)) \quad (4)$$

$$H(\lambda) \sim DP(\tau_0 H_0(\lambda)), \quad (5)$$

where  $DP(mC(x))$  denotes the Dirichlet process,<sup>33</sup> with mass parameter  $m$  and centering distribution  $C(x)$ . The distributions  $F$ ,  $G_0$ , and  $H_0$  are given as:

$$F((\phi_i, \psi_i) | \mu_i, \lambda_i) = N_2((\phi_i, \psi_i) | \mu_i, \lambda_i) \quad (6)$$

$$G_0(\mu) = N_2(\mu | \mu_0, \lambda_0) \quad (7)$$

$$H_0(\lambda) = W_{i2}(\lambda | \alpha_0, \beta_0), \quad (8)$$

where  $N_2(x | m, p)$  denotes the bivariate normal distribution, with mean  $m$  and variance  $p^{-1}$  for the random vector  $x$ , and  $W_{i2}(x | \alpha, \beta)$  denotes the two-dimensional Wishart distribution with mean  $\alpha/\beta$ .

Density estimation is accomplished by estimating  $\mu_i$ , the mean vector for the  $i$ th observation, and  $\lambda_i$ , the precision matrix (i.e., the inverse of the covariance matrix) for the  $i$ th observation. We fit the model using standard methods for Bayesian inference. In particular, we used Gibbs sampling to update the model parameters ( $\mu$ 's and  $\lambda$ 's) and updated the allocation of observations using the auxiliary Gibbs sampler with one auxiliary variable.<sup>34</sup>

### Parameter settings

The model described in Nonparametric Bayesian Density Estimation requires choosing values for the six hyperparameters. The mass parameters  $\eta_0$  and  $\tau_0$  were both set to 1 (implying, e.g., that, for  $n=94$ , the  $\mu$ 's and the  $\lambda$ 's will cluster into about 5.1 clusters each). The hyperparameter  $\mu_0$  is set to (0,0), and  $\lambda_0$  is a diagonal matrix whose elements are  $1/180^2$ . This provides for a diffuse centering distribution  $G_0(\mu)$ , since the most extreme angle of  $-180^\circ$  or  $180^\circ$  is only 1 SD from the mean. Finally,  $\alpha_0$  is set to 1, and  $\beta_0$  is a diagonal matrix whose diagonal elements are  $20^2$ . This provides for a diffuse centering distribution  $H_0(\lambda)$ .

Convergence was assessed by running two independent chains from initial states chosen from the prior states. The first 5000 iterations from each chain were discarded as burn-in, and output from the two chains was pooled to yield 40,000 samples.

### Predictive inference

From the Gibbs sampling output, the posterior predictive density of a new  $(\phi, \psi)$  pair was obtained.<sup>31</sup> Briefly, at each iteration of the sampler, new  $\mu$  and  $\lambda$  values were drawn from their posterior distribution, and the resulting multivariate normal density was evaluated on a fixed two-dimensional grid with steps of  $5^\circ$ . Averaging over the iterations yielded an estimate of the height of the joint density at that point. The conditional distribution of one of

the angles given the other was obtained by linear interpolation of the two closest sets of grid values. Figure 1 shows representative images of the bivariate density generated using our density estimation model.

Although this approach does not directly account for the periodic nature of torsion angle data, we are confident in our fits as most of the data are typically far away from the boundary at  $180^\circ/-180^\circ$ . At the boundary, we require two mixture components to model the data at the  $-180^\circ/180^\circ$  boundary. We are currently developing a newer model that will account for this periodicity (K. Lennox, D. Dahl, M. Vannucci & J. Tsai, Density estimation for protein conformation angles using a Bivariate von Mises distribution and Bayesian nonparametrics, unpublished results); however, initial comparisons show no strong differences for the data analyzed in this article besides needing an extra component to represent the density at this boundary.

### Distance of divergence

The similarity of two densities  $P$  and  $Q$  was assessed using the Jensen–Shannon divergence:

$$\frac{1}{2} \left( D_{KL} \left( P \parallel \frac{P+Q}{2} \right) + D_{KL} \left( Q \parallel \frac{P+Q}{2} \right) \right), \quad (9)$$

where

$$D_{KL}(P|Q) = \sum_i P(i) \log \frac{P(i)}{Q(i)}. \quad (10)$$

The minimum for the Jensen–Shannon divergence is 0 for exactly matching densities. Therefore, distances closer to 0 indicate that the two densities closely match, and those farther from 0 indicate that the two densities match poorly.

### Clustering

The density-estimated torsion angle distributions were clustered using the above Jensen–Shannon divergence score as distance. We used an agglomerative approach to clustering that only added a new member if its distance was lower than all others, which is in the same spirit as an average linkage clustering. This was performed because the distance divergence similarity is not associative. For example, A being similar to B and B being similar to C do not directly imply that A and C would also have a low divergence distance.

### Acknowledgements

We would like to acknowledge J. Bradley Holmes, Jerod Parsons, and Robert Bliss for help with the torsion angle calculations, as well as Chuck Staben for assistance with substitution matrices. J. Tsai, D. B. Dahl, and M. Vannucci were supported by National Institutes of Health/National Institute of General Medical Sciences grant R01GM81631. M. Vannucci was also supported by National Institutes of Health/National Human Genome Research Ins-

tute grant R01HG003319 and by National Science Foundation Division of Mathematical Sciences grant DMS-0605001.

### References

- Ramachandran, G. N., Ramakrishnan, C. & Sasisekharan, V. (1963). Stereochemistry of polypeptide chain configurations. *J. Mol. Biol.* **7**, 95–99.
- Kleywegt, G. J. & Jones, T. A. (1996). Phi/psi-chology: Ramachandran revisited. *Structure*, **4**, 1395–1400.
- Kleywegt, G. J. & Jones, T. A. (1998). Databases in protein crystallography. *Acta Crystallogr. Sect. D*, **54**, 1119–1131.
- Cornette, J., Cease, K. B., Margalit, H., Spouge, J. L., Berzofsky, J. A. & DeLisi, C. (1987). Hydrophobicity scales and computational techniques for detecting amphipathic structures in proteins. *J. Mol. Biol.* **195**, 659–685.
- Riddle, D. S., Santiago, J. V., Bray-Hall, S. T., Doshi, N., Grantcharova, V. P., Yi, Q. & Baker, D. (1997). Functional rapidly folding proteins from simplified amino acid sequences. *Nat. Struct. Biol.* **4**, 805–809.
- Walter, K. U., Vamvaca, K. & Hilvert, D. (2005). An active enzyme constructed from a 9-amino acid alphabet. *J. Biol. Chem.* **280**, 37742–37746.
- Chan, H. S. (1999). Folding alphabets. *Nat. Struct. Biol.* **6**, 994–996.
- Li, T., Fan, K., Wang, J. & Wang, W. (2003). Reduction of protein sequence complexity by residue grouping. *Protein Eng.* **16**, 323–330.
- Wang, J. & Wang, W. (1999). A computational approach to simplifying the protein folding alphabet. *Nat. Struct. Biol.* **6**, 1033–1038.
- Cannata, N., Toppo, S., Romualdi, C. & Valle, G. (2002). Simplifying amino acid alphabets by means of a branch and bound algorithm and substitution matrices. *Bioinformatics*, **18**, 1102–1108.
- Melo, F. & Marti-Renom, M. A. (2006). Accuracy of sequence alignment and fold assessment using reduced amino acid alphabets. *Proteins: Struct. Funct. Genet.* **63**, 986–995.
- Murphy, L. R., Wallqvist, A. & Levy, R. M. (2000). Simplified amino acid alphabets for protein fold recognition and implications for folding. *Protein Eng.* **13**, 149–152.
- Ogata, K., Ohya, M. & Umeyama, H. (1998). Amino acid similarity matrix for homology modeling derived from structural alignment and optimized by the Monte Carlo method. *J. Mol. Graphics Modell.*, **16**, 178–189, 254.
- Anderson, R. J., Weng, Z., Campbell, R. K. & Jiang, X. (2005). Main-chain conformational tendencies of amino acids. *Proteins: Struct. Funct. Genet.* **60**, 679–689.
- Kolaskar, A. S. & Kulkarni-Kale, U. (1992). Sequence alignment approach to pick up conformationally similar protein fragments. *J. Mol. Biol.* **223**, 1053–1061.
- Niefind, K. & Schomburg, D. (1991). Amino acid similarity coefficients for protein modeling and sequence alignment derived from main-chain folding angles. *J. Mol. Biol.* **219**, 481–497.
- Pal, D. & Chakrabarti, P. (2000). Conformational similarity indices between different residues in proteins and alpha-helix propensities. *J. Biomol. Struct. Dyn.* **18**, 273–280.
- Berman, H. M., Westbrook, J., Feng, Z., Gilliland, G., Bhat, T. N., Weissig, H. *et al.* (2000). The Protein Data Bank. *Nucleic Acids Res.* **28**, 235–242.

19. Levitt, M. (2007). Growth of novel protein structural data. *Proc. Natl Acad. Sci. USA*, **104**, 3183–3188.
20. Hovmoller, S., Zhou, T. & Ohlson, T. (2002). Conformations of amino acids in proteins. *Acta Crystallogr. Sect. D*, **58**, 768–776.
21. Lovell, S. C., Davis, I. W., Arendall, W. B., 3rd, de Bakker, P. I., Word, J. M., Prisant, M. G. *et al.* (2003). Structure validation by C $\alpha$  geometry: phi,psi and Cbeta deviation. *Proteins: Struct. Funct. Genet.* **50**, 437–450.
22. Pertselmidis, A., Zelinka, J., Fondon, J. W., 3rd, Henderson, R. K. & Otwinowski, Z. (2005). Bayesian statistical studies of the Ramachandran distribution. *Stat. Appl. Genet. Mol. Biol.* **4**; (Article 35).
23. Ho, B. K., Thomas, A. & Brasseur, R. (2003). Revisiting the Ramachandran plot: hard-sphere repulsion, electrostatics, and H-bonding in the alpha-helix. *Protein Sci.* **12**, 2508–2522.
24. Ramachandran, G. N. & Sasisekharan, V. (1968). Conformation of polypeptides and proteins. *Adv. Protein Chem.* **23**, 283–438.
25. Gunasekaran, K., Ramakrishnan, C. & Balaram, P. (1996). Disallowed Ramachandran conformations of amino acid residues in protein structures. *J. Mol. Biol.* **264**, 191–198.
26. Felsenstein, J. (2005). Version 3.6. Distributed by the author, Department of Genome Sciences, University of Washington, Seattle.
27. Henikoff, S. & Henikoff, J. G. (1992). Amino acid substitution matrices from protein blocks. *Proc. Natl Acad. Sci. USA*, **89**, 10915–10919.
28. Pauling, L. (1928). The shared-electron chemical bond. *Proc. Natl Acad. Sci. USA*, **14**, 359–362.
29. Wang, G. & Dunbrack, R. L. (2003). PISCES: a protein sequence culling server. *Bioinformatics*, **19**, 1589–1591.
30. Kabsch, W. & Sander, C. (1983). Dictionary of protein secondary structure: pattern recognition of hydrogen-bonded and geometrical features. *Biopolymers*, **22**, 2577–2637.
31. Escobar, M. D. & West, M. (1995). Bayesian density estimation and inference using mixtures. *J. Am. Stat. Assoc.* **90**, 577–588.
32. MacEachern, M. & Müller, P. (2000). Efficient meme schemes for robust model extensions using encompassing Dirichlet process mixture models. In *Robust Bayesian Analysis* (Insua, D. R. & Ruggeri, F., eds), pp. 295–315, Springer-Verlag Inc, New York, NY.
33. Ferguson, T. S. (1973). A Bayesian analysis of some nonparametric problems. *Ann. Stat.* **1**, 209–230.
34. Neal, R. M. (2000). Markov chain sampling methods for Dirichlet process mixture models. *J. Comput. Graph. Stat.* **9**, 249–265.